Absence of collective decay in a cold Rydberg gas

Tao Zhou, B. G. Richards, and R. R. Jones
Department of Physics, University of Virginia, Charlottesville, Virginia 22904-4714, USA
(Received 29 September 2015; revised manuscript received 7 January 2016; published 8 March 2016)

We have studied the decay of Rydberg excitations in a cold Rb gas. A 10 ns, pulsed-dye-amplified diode laser excites Rb atoms at 70 μK in a magneto-optical trap to ns or np Rydberg states with principal quantum numbers $26 \leqslant n \leqslant 40$. Time-delayed state-selective field ionization is used to directly monitor the population in the initial and neighboring Rydberg levels. The measured time dependence of the Rydberg population is well described by numerical simulations which consider only spontaneous emission and population transfer by blackbody radiation. No evidence for collective decay is found at atom densities up to 3×10^9 cm^{-3}. This result is in contrast to a previous study [Wang *et al.*, Phys. Rev. A **75**, 033802 (2007)], in which superradiant decay was theoretically predicted and experimentally inferred for atom density and laser focal volume conditions very similar to those considered here. Suppression of collective emission is likely due to variations in transition energies within the atom sample, dominated by inhomogeneities in dipole-dipole exchange interactions for initial s states, or by a combination of dipole-dipole and electric field inhomogeneities for the initial p states.

DOI: 10.1103/PhysRevA.93.033407

I. INTRODUCTION

Atoms within cold Rydberg ensembles are coupled by strong long-range dipole-dipole (DD) interactions [1], making them interesting systems for exploring few- and many-body quantum dynamics in general and applications in quantum information in particular [2–35]. Of course, unlike in ground-state systems, finite Rydberg lifetimes limit the types of measurements and number of coherent manipulations that can be performed in a given experiment. Fortunately, isolated Rydberg atoms exhibit low spontaneous decay rates [1], potentially enabling processing over micro- to millisecond time scales. At first glance this stability against radiative decay might seem surprising given the large transition matrix elements between adjacent Rydberg states, which scale as n^2. However, spontaneous decay to nearby levels via low-frequency emission is strongly suppressed by the ω^3 dependence of the Einstein A coefficient. As a result, the predominant decay path for isolated Rydberg atoms in low-angular-momentum states is to the ground or low-lying excited levels, resulting in an n^{-3} scaling of the spontaneous emission rate [1].

That said, neighboring Rydberg levels can play a dominant role in the decay of a large number N of atoms which either are simultaneously excited in a volume with dimensions smaller than the wavelength λ of the emitted light, or are sequentially excited throughout a cylindrical volume with length $L \gg \lambda$ [36,37]. In his seminal paper [38], Dicke predicted that a dense collection of N radiators, either in very close proximity or in a properly phased extended distribution, could develop spontaneous correlations and collectively emit radiation at rates greatly exceeding ("superradiance"), or much smaller than ("subradiance"), those of individuals in the sample. For the two-level systems considered by Dicke, correlations between a large number of emitting atoms can initiate collective superradiant emission at a per atom rate up to $N/4$ times larger than that between the same two levels in an isolated atom [38]. Collective emission remains a subject of considerable interest in many different contexts, including Rydberg atoms [39–51].

The presence of blackbody radiation, the existence of multiple photodecay channels in a Rydberg ladder, and strong DD interactions between atoms, all explicitly neglected in Dicke's original paper (and in many subsequent treatments) [38,52,53], make it much more difficult to observe, characterize, and quantitatively predict collective decay phenomena in Rydberg gases. In particular, DD interactions can suppress superradiance. In a thermal gas, this suppression results from DD-mediated collisions that homogeneously dephase the individual emitters in the ensemble at a rate greater than the superradiance rate [50]. In a frozen gas, DD exchange interactions couple pairs, or larger groups, of atoms leading to a variation in transition energies across the ensemble. Such inhomogeneities squelch the correlations that underlie superradiance, along with the collective emission [47]. That said, a clear signature of superradiance between Rydberg states, a fluorescence cascade from a Rydberg ladder proceeding at a rate much greater than spontaneous emission of isolated atoms, was first observed following pulsed-laser excitation of an elongated volume ($L \gg \lambda$) in a thermal cell [36]. More recently, direct evidence for superradiance was found in the millimeter-wave emission from a large cylindrical volume of Ca Rydberg atoms in a supersonic expansion, also with $L \gg \lambda$ [49,50]. As pointed out in the latter work, the rates for superradiant decay and DD dephasing within a given decay channel are essentially identical, up to a multiplicative geometric factor L/λ in the superradiance rate formula. Accordingly, it was suggested that collective decay should not play a major role in Rydberg depopulation unless $L \gg \lambda$ [50].

Still, despite competing DD effects, under certain conditions superradiance should play some role in cold ensembles where the dimensions of the excited volume are less than or comparable to λ. Indeed, evidence of reduced Rydberg lifetimes has been reported in several such experiments [39,48,51,54,55]. For example, Feng *et al.* observed a density-dependent lifetime suppression of Cs Rydberg atoms in a magneto-optical trap (MOT) [54]. They attribute the suppression to a combination of neutral Rydberg atom collisions and superradiance. However, the evidence for superradiance appears tenuous as their calculations with and without superradiant contributions both fall within their measurement uncertainty (see their Fig. 2). In addition, if one applies their

values for Rydberg collision velocity and cross section, the collisional depopulation rates are over three orders of magnitude too small to account for their observations. Han and Maeda attributed population transfer from initial to neighboring Rb Rydberg states to superradiance, but provided no evidence ruling out other possible population transfer mechanisms [56]. In other measurements, using fluorescence detection, Day *et al.* found Rydberg depopulation rates that were roughly twice that expected from single-atom spontaneous emission over a range of n states and at low densities, $\rho \sim 1 \times 10^7\,\mathrm{cm}^{-3}$ [48]. The small variation of the lifetime suppression with principal quantum number coupled with trap loss measurements argued against collisional depopulation and blackbody ionization. Instead, the enhanced Rydberg decay rate was found to be qualitatively consistent with a simplified collective decay model. In other experiments, the inclusion of superradiant decay channels was found to improve the quality of model fits to electromagnetically induced transparency measurements in cold Rydberg gases [51,55].

Certainly, a substantial decrease in Rydberg lifetimes due to collective emission would have a significant impact on most cold Rydberg atom experiments. Perhaps more important, in the context of the exploration and control of few- or many-body Rydberg dynamics, are the influences of the spontaneous quantum correlations that are predicted to develop with the emission of the first photon from the sample and evolve as the Rydberg population descends through a ladder of Dicke states [38,53]. Interestingly, Wang *et al.* presented a sophisticated theoretical treatment of photodecay in a multilevel Rydberg system which makes definite predictions as to whether superradiance should occur for a given initial principal quantum number, atom density, and experimental volume [39]. The theory apparently reproduced the rapid decay, at a rate approximately 40 times greater than predicted from spontaneous emission alone, of an initial population of 43p atoms in a MOT at a density of $\rho \sim 5 \times 10^8\,\mathrm{cm}^{-3}$.

We have used pulsed-laser excitation of Rb Rydberg atoms in a MOT under conditions ostensibly similar to those used in Ref. [39] in an attempt to test the predictions of their Rydberg superradiance theory. We employ state-selective field ionization (SSFI) to measure the population in the initial and neighboring Rydberg states as a function of delay after the laser excitation. We find no evidence for the predicted collective decay over a range of principal quantum numbers $26 \leqslant n \leqslant 40$ and atom densities $\rho \sim 3 \times 10^9\,\mathrm{cm}^{-3}$, despite the fact that, for these states, our highest density is more than two orders of magnitude above the predicted superradiance threshold [39]. Instead, our measurements are consistent with noncorrelated spontaneous decay combined with population redistribution via blackbody radiation.

II. EXPERIMENTAL PROCEDURE AND RESULTS

In the experiments, ^{85}Rb atoms at 70 μK are held in a MOT. The full width at half maximum (FWHM) diameter of the atom cloud is 0.4 mm. The MOT is positioned at the center of four parallel rods which facilitate the application of static and pulsed electric fields in the y direction for exciting and detecting Rydberg atoms in the MOT. A 10 ns pulsed, tunable, dye-amplified, ∼480 nm diode laser propagating in the x direction is focused into the center of the MOT, creating a cylindrically shaped volume of cold Rydberg atoms with a FWHM diameter of ∼0.1 mm and a length of 0.4 mm. The MOT and Rydberg lasers are non collinear, preventing the excitation of Rydberg atoms throughout any extended volume from the lower-density background of thermal Rb atoms in the chamber. The ∼100 MHz bandwidth of the Rydberg excitation laser ensures that there is no excitation suppression via dipole blockade [2,3]. At a variable time τ after the laser excitation, a ramped voltage is applied to two of the rods, ionizing any Rydberg atoms in the interaction region and pushing the resulting ions toward a microchannel plate (MCP) detector. Ions originating from different Rydberg states arrive at the detector at different times. The integrated signals in different time bins are proportional to the populations in different Rydberg states and are recorded for each laser shot as a function of the ionization time τ. The experiment proceeds at the 15 Hz dye-laser repetition rate.

The diode laser is tuned to selectively excite atoms from the upper $5p$ trap level to ns and np Rydberg states with $26 \leqslant n \leqslant 40$. Excitation of np states is facilitated by the application of a weak static electric field (from 30 V/cm at $n = 26$, 16 V/cm at $n = 32$, to 7 V/cm at $n = 40$). The density of $5p$ atoms in the MOT is determined, to within 30%, by combining measurements of the spatial dimensions of the atom cloud size via direct imaging with a CCD camera with measurements of the radiated fluorescence using an optical power meter. By saturating the Rydberg excitation using high laser fluence, we ensure that 50% of the $5p$ atoms within the interaction volume are excited to Rydberg states, enabling us to determine the Rydberg atom density [57]. Subsidiary experiments on resonant energy transfer between Rydberg atoms are consistent with the Rydberg density determination [57,58]. The MOT fluorescence is monitored throughout the lifetime measurements, ensuring that the number of atoms in the MOT is constant to within a few percent as τ is scanned. Care is taken to minimize the amplified spontaneous emission from the dye-amplified laser pulse, eliminating direct photoionization of $5p$ atoms. For the s-state measurements, a small, ∼1.5 V/cm, residual electric field persists in the interaction region due to imperfect shielding of the high-voltage-biased MCP (a larger field is present for initial p states). This field is sufficient to eject any ions or electrons from the interaction region, eliminating extended interactions between charged particles and neutral Rydberg atoms, and preventing the spontaneous evolution of the Rydberg gas into a plasma [59,60]. Neither the small static field employed for the p-state measurements nor the smaller residual field present during the s-state measurements substantially alters the rates for spontaneous emission or population transfer induced by blackbody radiation. The potential influence of the field inhomogeneity on superradiant decay is considered in the Analysis and Discussion section below.

Figures 1 and 2 show our principal experimental results. In Figs. 1(a) and 1(c), the probabilities for finding atoms in the $26s + 25p$, $32s$, and $40s$ states are plotted as functions of detection time τ for the maximum densities explored, $\rho \sim 3 \times 10^9\,\mathrm{cm}^{-3}$ and $\rho \sim 1.5 \times 10^9\,\mathrm{cm}^{-3}$, respectively. Note that for the lowest initial n state the sum of the $26s$ and $25p$ populations is shown since their corresponding features could not be

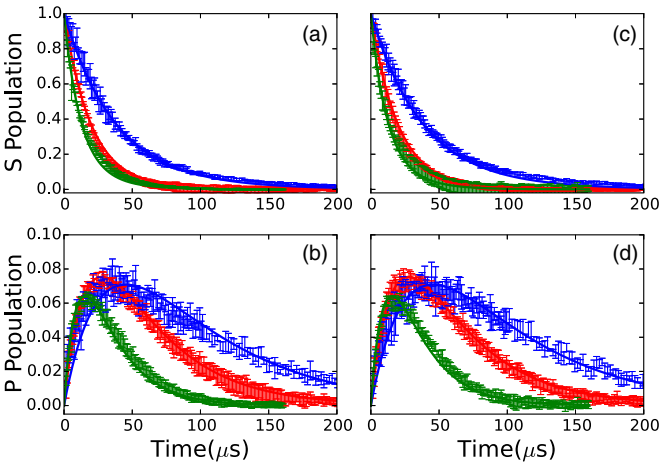

FIG. 1. (a),(c) Probabilities for finding atoms in $26s + 25p$ (green, fastest decay), $32s$ (red, intermediate decay), and $40s$ (blue, slowest decay) as a function of detection time τ for Rydberg densities of $\rho \sim 3 \times 10^9\,\mathrm{cm}^{-3}$ (a) and $\rho \sim 1.5 \times 10^9\,\mathrm{cm}^{-3}$ (c). Note that the sum of the $26s$ and $25p$ populations is shown since their corresponding features could not be adequately separated in the field-ionization signal. Vertical bars show the experimental data with uncertainties, and the solid curves are calculated as described in the text. Measurements and calculations for the $40s$ decay extend to 500 μs where the remaining population is negligible. (b),(d) Probabilities for finding atoms in $26p$ (green, fastest rise and decay), $32p$ (red, intermediate rise and decay), and $40p$ (blue, slowest rise and decay) levels as a function of detection time τ. The states are populated by blackbody redistribution from the initial $26s$, $32s$, and $40s$ levels, respectively. The data were measured simultaneously with those shown in (a) and (c). Vertical bars show the experimental data with uncertainties, and the solid curves are calculated as described in the text. The measured p-state probabilities are normalized to the calculations as described in the text. The calculations have no free parameters and consider only the effects of spontaneous emission and blackbody radiation on isolated atoms.

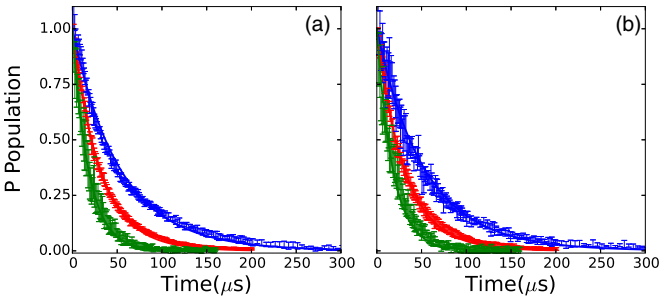

FIG. 2. Probabilities for finding atoms in $26p$ (green, fastest decay), $32p$ (red, intermediate decay), and $40p$ (blue, slowest decay) as functions of detection time τ for Rydberg densities of $\rho \sim 3 \times 10^9\,\mathrm{cm}^{-3}$ (a) and $\rho \sim 1.5 \times 10^9\,\mathrm{cm}^{-3}$ (b). Vertical bars show the experimental data with uncertainties, and the solid curves are calculated as described in the text. Measurements and calculations for the $40p$ decay extend to 500 μs where the remaining population is negligible. The calculations have no free parameters and consider only the effects of spontaneous emission and blackbody radiation on isolated atoms.

adequately separated in the time-resolved field-ionization signal. Within experimental uncertainties, the decays for the three initial s states are identical at the two densities shown. Additional measurements were made at Rydberg densities as low as $\rho \sim 2 \times 10^8\,\mathrm{cm}^{-3}$ (for $32s$ initial states) and $\rho \sim 5 \times 10^8\,\mathrm{cm}^{-3}$ (for $32p$ initial states), but no statistically significant differences were observed in the decays.

For spontaneous decay of isolated atoms at absolute zero, one would expect lifetimes of 28 and 58 μs for the $32s$ and $40s$ atoms, respectively [61]. The measured lifetimes for the $32s$ and $40s$ states are substantially smaller, 19 and 38 μs, respectively, due to population redistribution by blackbody radiation from the 300 K environment surrounding the MOT. Indeed, redistributed population is detected in neighboring Rydberg levels. In particular, Figs. 1(b) and 1(d) show the delay-dependent population in the p states ($26p$, $32p$, and $40p$) that lie immediately *above* the respective initial s states. Although we would expect to find some atoms in the adjacent, *lower-lying* p states as well, small features reflecting that population in the time-of-ionization signal lie within the initial-state peak (for the case of $26s$) or are masked by the tail of the larger, initial-state peak which precedes it.

The measured lifetime for the combined $26s + 25p$ states is 14 μs, the same as that expected from spontaneous decay of the $26s$ level alone [61]. Simulations (described in detail below) indicate that this apparent agreement is not due to the absence of blackbody transfer out of $26s$. Rather, the small longer-lived $25p$ component of the signal masks much of the change in the $26s$ decay, with a predicted effective lifetime of 13 μs for the $26s + 25p$ combination, similar to what we observe. We note that due to the slew rate of the ionizing field, there is a distribution of ionization times and, therefore, of detection efficiencies for atoms in different states. As a result, each of the measured p-state populations in Figs. 1(b) and 1(d) has been multiplied by a normalization factor to obtain the best agreement with the calculated decay curves that are shown in the figures and described in the next section.

Figure 2 shows analogous data for the decay of initially excited $26p$, $32p$, and $40p$ states. Again, due to blackbody redistribution, the lifetimes associated with these decays (18, 31, and 51 μs), are considerably smaller than expected from spontaneous emission alone (37, 75, and 155 μs) [61]. However, in this case, no substantial population is detected in the neighboring s or d levels. The analysis described in the next section indicates that the populations in these states are not detectable within our signal-to-noise ratio, remaining at or below the few percent level due to the relatively rapid spontaneous emission rate out of the s states, and smaller $p \rightarrow s$ and $p \rightarrow d$ blackbody transition rates.

III. ANALYSIS AND DISCUSSION

To determine if collective processes play any significant role in the decays we observe, we compare the measurements to the results of a simple rate equation model. The model includes population transfer via stimulated emission and absorption of blackbody radiation between an essential set of s, p, and d Rydberg states neighboring the initial level, as well as spontaneous emission out of those essential states to (undetected) lower-lying levels. We calculate the blackbody

transition rates between the essential states [1] as well as the known total spontaneous emission rates of the s, p, and d Rydberg levels [1].

For example, for an initially excited $40s$ state, the rate equation describing the time-dependent population in the initial $40s$ level is

$$\frac{dN_{40s}}{dt} = (-A_{40s} - B_{40s\to 40p} - B_{40s\to 39p})N_{40s} + B_{39p\to 40s}N_{39p} + B_{40p\to 40s}N_{40p} \quad (1)$$

where $N_{n\ell}$ is the population in state $n\ell$, A_{40s} is the $40s$ spontaneous decay rate, and $B_{n\ell\to n'\ell'}$ is the blackbody transition rate from $n\ell$ to $n'\ell'$ [1]:

$$B_{n\ell\to n'\ell'} = 2\bar{n}\alpha^3\omega^2_{n\ell,n'\ell'}|\bar{f}_{n\ell,n'\ell'}|. \quad (2)$$

In Eq. (2), $\bar{n} = (e^{\omega_{n\ell,n'\ell'}/kT} - 1)^{-1}$ is the photon occupation number at the frequency $\omega_{n\ell,n'\ell'}$ corresponding to the energy splitting between states $n\ell$ and $n'\ell'$, k is Boltzmann's constant, T is the temperature, α is the fine-structure constant, and $|\bar{f}_{n\ell,n'\ell'}|$ is the magnitude of the oscillator strength averaged over all orientations of the initial and final states $n\ell$ and $n'\ell'$. We use the spontaneous emission rates calculated by Gounand [61].

The populations in the secondary states $39p$ and $40p$ are computed using similar rate equations that include the total spontaneous decay rate out of those levels as well as blackbody transitions to and from pairs of s and d levels that lie immediately above and below each p state. We truncate the system of equations with rate equations that include spontaneous decay from the tertiary s and d levels and their blackbody couplings with the secondary states. Analogous systems of equations are used to compute the Rydberg population decay following initial p-state excitation. We note that, for initial or intermediate p states in particular, blackbody radiation redistributes a small, but non-negligible, fraction of the initial population beyond the nearest-neighbor s and d states. Therefore, an approximate expression [1]

$$B_{n\ell} = \frac{4\alpha^3 kT}{3n^2} \quad (3)$$

for the total blackbody decay rate from each p level is used to more accurately account for the net transfer out of these states.

The results of our calculation, which ignore any collective decay phenomena, are shown with the data in Figs. 1 and 2. Overall, the agreement is reasonable. Aside from the previously noted renormalization of the experimental p-state population, no parameter adjustments have been made to obtain the level of agreement shown. The data provide no evidence of a significant reduction in the Rydberg lifetimes due to superradiance. This is true over a range of principal quantum numbers and atom densities where superradiant emission has been predicted to be the dominant decay path [39].

It is well established that superradiance is suppressed by inhomogeneities in transition energies across a sample of emitters [47], and we suspect that this is the case in our, and many other, cold atom experiments. In our experiments, three different effects contribute to such inhomogeneities. The first, and dominant mechanism for some of our measurements, is the DD exchange interaction. Consider a pair of identical atoms with two levels s and p and interatomic separation R. Spontaneous emission from the initial upper pair state ss results in the population of the bright configuration of the lower-energy pair state $(sp + ps)/\sqrt{2}$. However, due to the DD coupling between the atoms, $V_{\rm DD} \propto |\langle s|r|p\rangle|^2/R^3$, the energy of this state is not the same as that for two atoms at infinite separation [1]. Accordingly, in a large ensemble of randomly spaced atoms, every possible configuration of N_s s atoms and N_p p atoms has a different energy, depending on the separation (and relative orientation) between the p atoms and their neighboring s atoms. As a result, any Dicke state, the bright linear combination of all possible configurations of N_s s atoms and N_p p atoms [38], is nonstationary. The phases of the constituent N-atom product states evolve at different rates, as determined by their DD energy shifts relative to their energies at infinite separation. The emission from these nonstationary Dicke states dephases at a rate comparable to the typical dipole-dipole energy shift $\bar{V_{\rm DD}}$ for pairs of atoms in the ensemble. Superradiance cannot occur unless the system transitions down each step in the Dicke ladder more rapidly than this dephasing. A similar argument has been made by Gross and Haroche [62]. In the frequency domain, atoms with different transition energies at different locations in the ensemble do not collectively emit into the same field unless that emission occurs in a very short burst with a sufficiently broad, coherent bandwidth.

To determine the DD dephasing rate, we use the most probable nearest-neighbor separation in a random ensemble, $R \simeq (2\pi\rho)^{-1/3}$, and average over all orientations of the Rydberg states on any two neighboring atoms ns and $n'p$ to obtain [63,64]

$$\bar{V_{\rm DD}} = \frac{8\pi}{9}\rho|\langle ns|r|n'p\rangle|^2. \quad (4)$$

Using a numerical Numerov integration algorithm to compute the relevant radial matrix elements [65], at the highest density studied ($\rho = 3\times 10^9\,{\rm cm}^{-3}$) we obtain values for the DD exchange coupling between the ns and $(n-1)p$ states, $\bar{V_{\rm DD}} = 2.4$, 6.2, and 17 MHz, for $n = 26$, 32, and 40, respectively. These interaction strengths set effective lower limits for the rates at which collective emission from ns to $(n-1)p$ can occur. Similarly, for initial np states and $\rho = 3\times 10^9\,{\rm cm}^{-3}$, the relevant exchange coupling is to the nearest lower-lying s states, with $\bar{V_{\rm DD}} = 3.1$, 7.8, and 20 MHz, for $n = 26$, 32, and 40, respectively.

The magnetic field gradient in the MOT is another source of energy inhomogeneities in our ensemble. As in Ref. [39], the magnetic field remains on during our measurements, resulting in a transition energy variation of approximately 1 MHz across the MOT. This inhomogeneity is smaller, or much smaller, than that due to dipole-dipole interactions at sufficiently high densities. It should not play a principal role in suppressing superradiance under the conditions used to produce Figs. 1 and 2.

The third contributor to the Rydberg energy variations across the ensemble is electric field inhomogeneity. While the voltages applied to the field rods produce a field that is quite uniform over the MOT (predicted field variations of 0.07%, corresponding to 21 mV/cm for the largest applied field of 30 V/cm for the $26p$ measurements) the residual field from the MCP is not as uniform. Using a combination

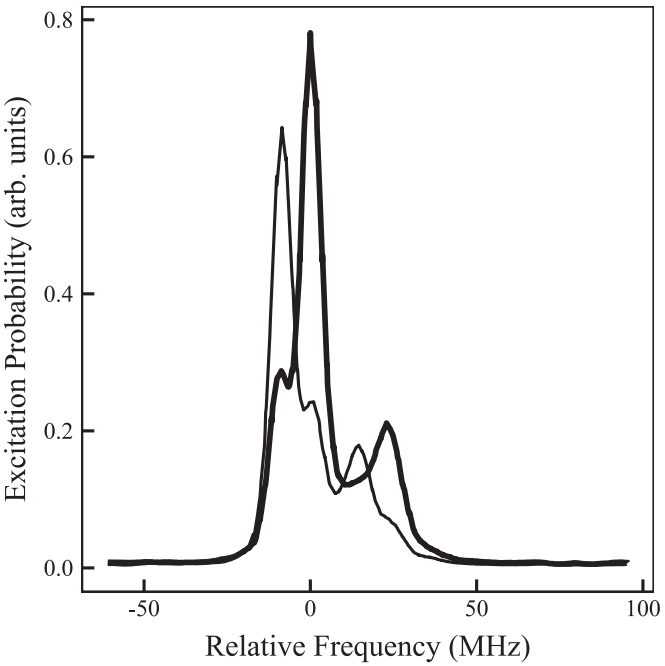

FIG. 3. Measured $32p_{3/2}$ $|m_j| = 1/2$ (bold line) and $|m_j| = 3/2$ (thin line) excitation probabilities as a function of Rydberg laser frequency in zero applied field. The two data curves are obtained simultaneously in the same laser frequency scan. The small feature on the left (right) of the main $|m_j| = 1/2$ (3/2) peak is the result of imperfect discrimination of the $|m_j| = 1/2$ and 3/2 components via SSFI. The additional peak on the right of the main feature in each trace is due to the trap-laser dressing of the $5p_{3/2}$ and $5s$ levels. Its frequency shift from the main peak reflects the Autler-Townes splitting of the $5p_{3/2}$ initial state.

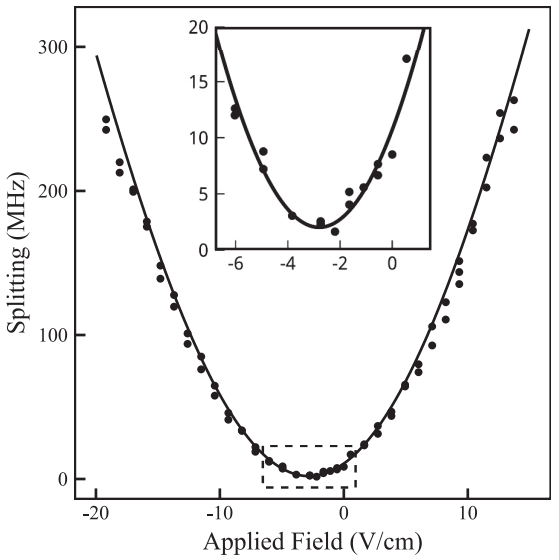

FIG. 4. Difference (i.e., splitting) in the transition energies for exciting $32p_{3/2}$ $|m_j| = 1/2,3/2$ from $5p_{3/2}$ as a function of applied electric field. Filled circles are measurements and the solid curve is the result of a numerical Stark map calculation assuming orthogonal "offset" and "residual" electric field components due to the MCP of 2.8 and 1.5 V/cm, respectively. The inset shows a magnified view of the portion of the main figure within the dashed window.

of spectroscopic measurements and accurate Stark energy calculations, we determine an upper limit for the Rydberg energy inhomogeneity due to the nonuniformity of the electric field F in the interaction region.

First, we measure the transition frequencies for excitation of $32p_{3/2}$ $|m_j| = 1/2,3/2$, from the $5p_{3/2}$ upper trap state as a function of the voltage applied to the field rods (see Fig. 3). For convenience, in the following discussion we refer to the field produced by the rods as the "applied" field. The experimental geometry is identical to that used for the lifetime measurements, but the Rydberg excitation is performed with an unamplified, 3 μs pulse chopped from the $\sim$1 MHz bandwidth cw diode laser. The Rydberg excitation pulse has $\sim$1 μs rise and fall times and is formed using an acousto-optic modulator. We use a temperature- and pressure-stabilized Fabry-Pérot interferometer to track the relative frequency of the Rydberg laser as it is scanned. The population in $|m_j| = 1/2$ is distinguished from that in $|m_j| = 3/2$ using SSFI. By recording the signal in two different time bins we obtain (nominally) separate excitation profiles to the two $|m_j|$ states in the same laser frequency scan. Therefore, the energy splitting between the two m_j states can be accurately determined to well within the excitation bandwidth which is dominated by the 6.07 MHz natural linewidth of the initial $5p_{3/2}$ level.

In zero electric field, the excitation profiles associated with the population in the two $|m_j|$ levels should exhibit maxima at the same laser frequency, i.e., have zero energy splitting. However, as shown in Fig. 4, we observe a minimum splitting of 2 MHz at an applied field of -2.8 V/cm. The minimum splitting at nonzero applied field allows us to determine the components of the MCP field parallel and perpendicular to applied field. Apparently, the application of a -2.8 V/cm rod field minimizes the net field in the interaction region. Accordingly, there must be a parallel, 2.8 V/cm, MCP field component which we call the "offset" field. Using the variation in the $|m_j|$ splitting as a function of applied field, we can also extract a value, 1.5 V/cm, for the perpendicular, i.e., "residual," MCP field component. The solid curve shown with the data in Fig. 4 is the predicted $32p_{3/2}$ $|m_j| = 1/2,3/2$ splitting as a function of applied field (extracted from a full numerical Stark map calculation based on the method of Zimmerman *et al.* [65]), assuming MCP offset and residual fields of 2.8 and 1.5 V/cm, respectively. The good agreement with experiment confirms the accuracy of the calculation as well as the offset and residual field determinations.

At, and near, the minimum splitting (i.e., in the presence of the residual field alone where the s-state decay measurements are performed), the $|m_j|$ excitation resonances have minimum linewidths of 8 MHz (see Fig. 3). As noted above, the predominant contribution to this linewidth is the 6.07 MHz natural width of the $5p_{3/2}$ level. However, the laser bandwidth, Zeeman shifts due to magnetic field inhomogeneities, and Stark shifts due to inhomogeneities in the 1.5 V/cm residual field also contribute. Assuming that the laser spectrum and field distributions are Gaussian, we deconvolute the primary line shape as a Voigt profile, and extract a bandwidth of

3.9 MHz for the total Gaussian contribution. Accordingly, we obtain an *upper-limit* estimate for the electric field inhomogeneity by assuming it is the sole contributor to this width. From the Stark shift of the $32p_{3/2}$ $m_j = 1/2$ level, $\Delta E = [6.5\ \text{MHz/(V/cm)}^2]F^2$, we determine that the maximum possible variation of the residual field across the interaction region is $\Delta F_{\text{res}} = 0.20$ V/cm. Using this field inhomogeneity with the field-dependent Stark shifts of the respective levels, we can compute the maximum range of transition energies between the initial s states and the p states immediately below them (to which the dipole coupling is the strongest). For the $26s \rightarrow 25p$, $32s \rightarrow 31p$, and $40s \rightarrow 39p$ transitions, the maximum energy variations across the excitation region (with only the residual field present) are 0.43, 2.2, and 12 MHz, respectively. The transition energy variations are smaller for transitions to lower lying p states due to the n^7 scaling of the Rydberg polarizability. So, at the highest densities we have explored, the energy inhomogeneities associated with the residual electric field are less, or much less, than those associated with the dipole-dipole exchange interaction. Therefore, the electric field inhomogeneities do not hold the primary responsibility for the suppression of superradiance from any of the initial s states.

The situation with the initial p states is somewhat different, as they are excited in a nonzero applied field that is considerably larger than the orthogonal residual field. As a result, the residual field and its inhomogeneity have essentially no effect on the transition energies. However, the spatial variations in the MCP offset field, which is parallel to the applied field, cannot be neglected. We use measurements of DD-mediated resonant energy transfer between Rydberg atoms to obtain an upper-limit estimate for the offset field inhomogeneity. Those experiments use the same experimental geometry as the Rydberg decay measurements [58,64]. In the experiments, the probability for resonant population transfer from one pair of Rydberg states to another (e.g., $25s + 33s \rightarrow 24p + 34p$ [64]) is recorded as a function of an applied field which Stark-tunes the total energies of the atom pair in the two different configurations. In a uniform field, the line shape describing the field-dependent energy transfer probability is characterized by a peak at the "resonance" condition, where the total energies of the two sets of atom pair states are identical, and a width that is proportional to the Rydberg density. In a nonuniform field, the line shape has a nonzero minimum width as the density approaches zero, due to variations in the local field at different locations within the sample. Consider the $25s + 33s \rightarrow 24p + 34p$ resonance [64] for which maximum population transfer occurs in an electric field of $F \sim 3.4$ V/cm. Assuming that the nonzero resonance width that is observed at very low Rydberg density [64] is due solely to the inhomogeneity in the electric field (i.e., ignoring magnetic field inhomogeneities and any other broadening effects) we obtain the maximum possible variation in the offset field, $\Delta F_{\text{off}} = 0.08$ V/cm, across the Rydberg sample. As an additional check, we consider a different energy transfer resonance, $32p + 32p \rightarrow 33s + 32s$, that is centered at a substantially higher field $F \sim 11.5$ V/cm [58]. The nonzero low-density width for this energy transfer resonance gives the same maximum value for the offset field inhomogeneity, $\Delta F_{\text{off}} = 0.08$ V/cm.

Given ΔF_{off}, we can compute the maximum possible variations in the energies, associated with transitions between initial p states and the nearest lower-lying s state, due to the inhomogeneous field. Using ΔF_{off}, the calculated Stark shifts of each of the states involved in the transitions $26p \rightarrow 26s$, $32p \rightarrow 32s$, and $40p \rightarrow 40s$, and the applied fields employed for the respective p-state excitations, we obtain the maximum possible transition energy variations due to the inhomogeneous electric field. These are 4.9, 13, and 30 MHz for the $26p$, $32p$, and $40p$ initial states, respectively. Accordingly, for the p-state decays, the maximum energy variations due to the field are comparable to, but up to a factor of $1.7\times$ larger than, those due to dipole-dipole interactions. Given our likely overestimate of the field inhomogeneity, both may play a role in suppressing collective emission from the ensemble.

IV. CONCLUSION

We have studied the decay of Rydberg excitations in a cold Rb gas and find no evidence for the dramatic decrease in lifetimes predicted by Wang *et al.* [39]. The decay rates and population redistribution we observe are consistent with a model that considers only spontaneous emission from, and blackbody redistribution within, isolated atoms. In our experiments, a small electric field in the interaction region ejects any free electrons or ions from the excitation volume, preventing ionization or population transfer due to interactions with charged particles. In addition, the lack of spatial overlap between the trapping lasers and the Rydberg excitation laser well outside of the cold atom cloud ensures that there is no Rydberg excitation within an extended volume of lower-density, background Rb atoms in the chamber. Suppression of superradiant emission is likely due to variations in transition energies across the cold Rydberg atom sample. For initial s states, these variations are dominated by inhomogeneities in DD exchange interactions within the random ensemble. Such inhomogeneities will necessarily be present in any measurement involving a large number of atoms where the separation between atoms is not well defined. For initial p states, the suppression is likely due to a combination of DD exchange and electric field inhomogeneities.

ACKNOWLEDGMENTS

It is a pleasure to acknowledge helpful conversations with T. F. Gallagher and F. Robicheaux. This work has been supported by the National Science Foundation.

[1] T. F. Gallagher, *Rydberg Atoms*, 1st ed. (Cambridge University Press, Cambridge, 1994).

[2] M. D. Lukin, M. Fleischhauer, R. Cote, L. M. Duan, D. Jaksch, J. I. Cirac, and P. Zoller, Phys. Rev. Lett. **87**, 037901 (2001).

[3] D. Tong, S. M. Farooqi, J. Stanojevic, S. Krishnan, Y. P. Zhang, R. Cote, E. E. Eyler, and P. L. Gould, Phys. Rev. Lett. **93**, 063001 (2004).

[4] F. Robicheaux and J. V. Hernandez, Phys. Rev. A **72**, 063403 (2005).

[5] T. Cubel Liebisch, A. Reinhard, P. R. Berman, and G. Raithel, Phys. Rev. Lett. **95**, 253002 (2005).

[6] T. Vogt, M. Viteau, J. Zhao, A. Chotia, D. Comparat, and P. Pillet, Phys. Rev. Lett. **97**, 083003 (2006).

[7] E. Urban, T. A. Johnson, T. Henage, L. Isenhower, D. D. Yavuz, T. G. Walker, and M. Saffman, Nat. Phys. **5**, 110 (2009).

[8] Alpha Gaëtan, Yevhen Miroshnychenko, Tatjana Wilk, Amodsen Chotia, Matthieu Viteau, Daniel Comparat, Pierre Pillet, Antoine Browaeys, and Philippe Grangier, Nat. Phys. **5**, 115 (2009).

[9] T. Wilk, A. Gaetan, C. Evellin, J. Wolters, Y. Miroshnychenko, P. Grangier, and A. Browaeys, Phys. Rev. Lett. **104**, 010502 (2010).

[10] Hendrik Weimer, Robert Low, Tilman Pfau, and Hans Peter Buchler, Phys. Rev. Lett. **101**, 250601 (2008).

[11] M. Saffman and K. Molmer, Phys. Rev. Lett. **102**, 240502 (2009).

[12] Robert Low, Hendrik Weimer, Ulrich Krohn, Rolf Heidemann, Vera Bendkowsky, Bjorn Butscher, Hans Peter Buchler, and Tilman Pfau, Phys. Rev. A **80**, 033422 (2009).

[13] T. Pohl and P. R. Berman, Phys. Rev. Lett. **102**, 013004 (2009).

[14] Thomas Amthor, Christian Giese, Christoph S. Hofmann, and Matthias Weidemuller, Phys. Rev. Lett. **104**, 013001 (2010).

[15] T. Pohl, E. Demler, and M. D. Lukin, Phys. Rev. Lett. **104**, 043002 (2010).

[16] S. Wuster, C. Ates, A. Eisfeld, and J. M. Rost, Phys. Rev. Lett. **105**, 053004 (2010).

[17] Jens Honer, Hendrik Weimer, Tilman Pfau, and Hans Peter Buchler, Phys. Rev. Lett. **105**, 160404 (2010).

[18] J. D. Pritchard, D. Maxwell, A. Gauguet, K. J. Weatherill, M. P. A. Jones, and C. S. Adams, Phys. Rev. Lett. **105**, 193603 (2010).

[19] A. Schwarzkopf, R. E. Sapiro, and G. Raithel, Phys. Rev. Lett. **107**, 103001 (2011).

[20] S. Sevincli, N. Henkel, C. Ates, and T. Pohl, Phys. Rev. Lett. **107**, 153001 (2011).

[21] F. Bariani, Y. O. Dudin, T. A. B. Kennedy, and A. Kuzmich, Phys. Rev. Lett. **108**, 030501 (2012).

[22] Matthieu Viteau, Paul Huillery, Mark G. Bason, Nicola Malossi, Donatella Ciampini, Oliver Morsch, Ennio Arimondo, Daniel Comparat, and Pierre Pillet, Phys. Rev. Lett. **109**, 053002 (2012).

[23] D. D. Bhaktavatsala Rao and Klaus Mølmer, Phys. Rev. Lett. **111**, 033606 (2013).

[24] H. Schempp, G. Gunter, M. Robert-de-Saint-Vincent, C. S. Hofmann, D. Breyel, A. Komnik, D. W. Schonleber, M. Garttner, J. Evers, S. Whitlock, and M. Weidemuller, Phys. Rev. Lett. **112**, 013002 (2014).

[25] Matthew Ebert, Alexander Gill, Michael Gibbons, Xianli Zhang, Mark Saffman, and Thad G. Walker, Phys. Rev. Lett. **112**, 043602 (2014).

[26] D. Paredes-Barato and C. S. Adams, Phys. Rev. Lett. **112**, 040501 (2014).

[27] H. Gorniaczyk, C. Tresp, J. Schmidt, H. Fedder, and S. Hofferberth, Phys. Rev. Lett. **113**, 053601 (2014).

[28] Daniel Tiarks, Simon Baur, Katharina Schneider, Stephan Dürr, and Gerhard Rempe, Phys. Rev. Lett. **113**, 053602 (2014).

[29] David Petrosyan and Klaus Molmer, Phys. Rev. Lett. **113**, 123003 (2014).

[30] J. Pellegrino, R. Bourgain, S. Jennewein, Y. R. P. Sortais, A. Browaeys, S. D. Jenkins, and J. Ruostekoski, Phys. Rev. Lett. **113**, 133602 (2014).

[31] Daniel Barredo, Henning Labuhn, Sylvain Ravets, Thierry Lahaye, Antoine Browaeys, and Charles S. Adams, Phys. Rev. Lett. **114**, 113002 (2015).

[32] Y. O. Dudin and A. Kuzmich, Science **336**, 887 (2012).

[33] Alexander W. Glaetzle, Marcello Dalmonte, Rejish Nath, Christian Gross, Immanuel Bloch, and Peter Zoller, Phys. Rev. Lett. **114**, 173002 (2015).

[34] R. M. W. van Bijnen and T. Pohl, Phys. Rev. Lett. **114**, 243002 (2015).

[35] M. Ebert, M. Kwon, T. G. Walker, and M. Saffman, Phys. Rev. Lett. **115**, 093601 (2015).

[36] F. Gounand, M. Hugon, P. R. Fournier, and J. Berlande, J. Phys. B **12**, 547 (1979).

[37] C. Carr, R. Ritter, C. G. Wade, C. S. Adams, and K. J. Weatherill, Phys. Rev. Lett. **111**, 113901 (2013).

[38] R. H. Dicke, Phys. Rev. **93**, 99 (1954).

[39] T. Wang, S. F. Yelin, R. Cote, E. E. Eyler, S. M. Farooqi, P. L. Gould, M. Kostrun, D. Tong, and D. Vrinceanu, Phys. Rev. A **75**, 033802 (2007).

[40] N. Skribanowitz, I. P. Herman, J. C. MacGillivray, and M. S. Feld, Phys. Rev. Lett. **30**, 309 (1973).

[41] M. Gross, C. Fabre, P. Pillet, and S. Haroche, Phys. Rev. Lett. **36**, 1035 (1976).

[42] D. Pavolini, A. Crubellier, P. Pillet, L. Cabaret, and S. Liberman, Phys. Rev. Lett. **54**, 1917 (1985).

[43] M. G. Moore and P. Meystre, Phys. Rev. Lett. **83**, 5202 (1999).

[44] J. I. Kim, R. B. B. Santos, and P. Nussenzveig, Phys. Rev. Lett. **86**, 1474 (2001).

[45] C. Greiner, B. Boggs, and T. W. Mossberg, Phys. Rev. Lett. **85**, 3793 (2000).

[46] Chiu Fan Lee and Neil F. Johnson, Phys. Rev. Lett. **93**, 083001 (2004).

[47] Vasily V. Temnov and Ulrike Woggon, Phys. Rev. Lett. **95**, 243602 (2005).

[48] J. O. Day, E. Brekke, and T. G. Walker, Phys. Rev. A **77**, 052712 (2008).

[49] Kirill Prozument, Anthony P. Colombo, Yan Zhou, G. B. Park, Vladimir S. Petrović, Stephen L. Coy, and Robert W. Field, Phys. Rev. Lett. **107**, 143001 (2011).

[50] Anthony P. Colombo, Yan Zhou, Kirill Prozument, Stephen L. Coy, and Robert W. Field, J. Chem. Phys. **138**, 014301 (2013).

[51] Florian Karlewski, Markus Mack, Jens Grimmel, Nora Sandor, and Jozsef Fortagh, Phys. Rev. A **91**, 043422 (2015).

[52] N. E. Rehler and J. H. Eberly, Phys. Rev. A **3**, 1735 (1971).

[53] R. Bonifacio and L. A. Lugiato, Phys. Rev. A **11**, 1507 (1975).

[54] Zhi-Gang Feng, Lin-Jie Zhang, Jian-Ming Zhao, Chang-Yong Li, and Suo-Tang Jia, J. Phys. B **42**, 145303 (2009).

[55] K. J. Weatherill, J. D. Pritchard, R. P. Abel, M. G. Bason, A. K. Mohapatra, and C. S. Adams, J. Phys. B **41**, 201002 (2008).

[56] Jianing Han and H. Maeda, Can. J. Phys. **92**, 1130 (2014).

[57] M. R. Kutteruf, Ph.D. thesis, University of Virginia, 2010.

[58] B. G. Richards and R. R. Jones (unpublished).

[59] Wenhui Li, Michael W. Noel, Michael P. Robinson, Paul J. Tanner, Thomas F. Gallagher, Daniel Comparat, Bruno Laburthe Tolra, Nicolas Vanhaecke, Thibault Vogt, Nassim Zahzam,

Pierre Pillet, and Duncan A. Tate, Phys. Rev. A **70**, 042713 (2004).
[60] M. P. Robinson, Ph.D. thesis, University of Virginia, 2002.
[61] F. Gounand, J. Phys. (Paris) **40**, 457 (1979).
[62] M. Gross and S. Haroche, Phys. Rep. **93**, 301 (1982).
[63] M. R. Kutteruf and R. R. Jones, Phys. Rev. A **82**, 063409 (2010).
[64] M. R. Kutteruf and R. R. Jones, Phys. Rev. Lett. **108**, 013001 (2012).
[65] M. L. Zimmerman, M. G. Littman, M. M. Kash, and D. Kleppner, Phys. Rev. A **20**, 2251 (1979).